ELSEVIER

Ceramics International 31 (2005) 1123–1130

CERAMICS INTERNATIONAL

www.elsevier.com/locate/ceramint

Processing and characterization of sol–gel fabricated mixed metal aluminates

M. Chroma [a], J. Pinkas [a,*], I. Pakutinskiene [b], A. Beganskiene [b], A. Kareiva [b,*]

[a] Department of Inorganic Chemistry, Masaryk University Brno, Kotlarska 2, CZ-61137 Brno, Czech Republic
[b] Department of General and Inorganic Chemistry, Vilnius University, Naugarduko 24, LT-01513 Vilnius, Lithuania

Received 25 July 2004; received in revised form 13 October 2004; accepted 22 November 2004
Available online 17 February 2005

Abstract

Nanocrystalline lanthanum aluminate ($LaAlO_3$, LAP) and Sr-substituted LAP ceramics were synthesized by sol–gel processes using mixtures of inorganic salts of the respective elements. The metal ions, generated by dissolving metal nitrates or acetates in acetic acid and/or water were complexed by 1,2-ethanediol to obtain the precursor for LAP. The XRD patterns of the $LaAlO_3$ and $La_{1-x}Sr_xAlO_{3-\delta}$ ($x \leq 0.50$) ceramic sintered at 1000 °C were almost identical with the perovskite LAP composition. The phase transformations, composition and microstructural features in the gels and polycrystalline samples were studied by thermal analysis (TG/DTA), powder X-ray diffraction analysis (XRD), infrared spectroscopy (IR), scanning electron microscopy (SEM), energy dispersive X-ray analysis (EDX) and inductively coupled argon plasma emission spectroscopy (ICP). The quality of the resulting products (homogeneity, crystallisation temperature, grain size and grain size distribution, etc.) of the "*chimie douce*" synthetic route is discussed.

Keywords: A. Powders: chemical preparation; A. Sol–gel processes; D. Perovskites

1. Introduction

The development of innovative multi-functional advanced materials should have a major impact in future applications. Ceramics based on Ln_2O_3–Al_2O_3 (Ln: lanthanide element) combination are promising materials for optical, electronic and structural applications [1–8]. The perovskite yttrium aluminate ($YAlO_3$, YAP) doped with lanthanide element offers advantages of longer lifetimes and higher, polarized cross sections with respect to most of other oxide matrices [9], and is useful as host for solid-state lasers, luminescence systems and window materials for a variety of lamps [10]. $LaAlO_3$ (LAP) and related materials are currently being incorporated into automobile catalytic converters [11]. $LaAlO_3$ is promising substrate for the epitaxy of thin oxide films and has potential use as a buffer layer for the epitaxial growth of various perovskite-type films such as a high temperature superconductors, ferroelectrics and colossal magnetoresistance oxides [12,13]. Owing to such a wide and diverse application potential of aluminate-based ceramics, new routes for the synthesis of various pure and homogeneously doped orthoaluminates are highly desirable.

The solid-state synthesis of different aluminates from oxide powders usually requires extensive mechanical mixing and lengthy heat treatments in the temperature range of 1300–1600 °C [8,14]. These processing conditions, however, do not allow a facile control over the microstructure, grain size and grain size distribution in the resulting powders or monoliths. Several wet-chemical and/or soft chemistry techniques, such as the polymerized complex route [2], combustion synthesis [3], homogeneous precipitation method [10], spray-drying preceramic processing [15], or base-catalyzed sol–gel process [16] have been used to produce aluminate phases. Most of these methods suffer from the complex and time-consuming procedures (long refluxing times, gelation periods of several days, etc.)

* Corresponding author. Tel.: +370 5 2336214; fax: +370 5 2330987.
E-mail address: aivaras.kareiva@chf.vu.lt (A. Kareiva).

0272-8842/$30.00
doi:10.1016/j.ceramint.2004.11.012

and/or mismatch in the solution behaviour of the constituents. As a consequence, gross inhomogeneities may be present in the obtained ceramics, e.g. significant amounts of impurity phases may form. The sol–gel methods based on molecular precursors have a cutting edge over the other solution routes because they allow chemical interactions among the precursor species of the initial mixture favoring the evolution of a homogeneous solid-state structure at the atomic level [17].

The unique properties of most of the mixed-cation oxide ceramics depend largely on impurities or dopants. Such complex oxides with the perovskite structure also demonstrate an impressive range of electrical, optical and magnetic properties. These properties of perovskites can be tuned by substituting cations at both sites. For instance, recently the strong photoluminescence was obtained without luminance temperature-degradation in the mixed alkaline earth substituted lanthanide aluminates or lanthanide doped alkaline earth aluminates [14,16,18–21]. Strontium atoms can substitute into the perovskite $LnAlO_3$ structure possibly for the lanthanide cation [22].

In the context of doped materials, the incorporation of homogeneously distributed nanosized secondary phases in a host matrix, which can be realized by the molecular level fabrication of new materials, is of significant interest. Over the last few decades, the sol–gel techniques have been used to prepare a variety of mixed-metal oxides [23–25]. In these sol–gel processes, good quality of the oxide products was achieved primarily because of the purity of the precursor materials used and chemical homogeneity obtained from the synthesis route. In this paper we present results of a systematic study of sol–gel synthetic approach to pure $LaAlO_3$ and Sr-substituted lanthanum aluminates $La_{1-x}Sr_xAlO_{3-\delta}$ using glycolate intermediates. The results illustrate the simplicity of the low-temperature method for the preparation of this type of ceramics. The formation of possible solid solutions in the investigated systems is discussed as well.

2. Experimental

Lanthanum aluminate ($LaAlO_3$; sample I) and lanthanum–strontium aluminate ($La_{0.75}Sr_{0.25}AlO_{3-\delta}$; sample II; $La_{0.50}Sr_{0.50}AlO_{3-\delta}$; sample III; $La_{0.25}Sr_{0.75}AlO_{3-\delta}$; sample IV) ceramic samples were synthesized by aqueous sol–gel method. The gels were prepared using stoichiometric amounts of analytical-grade $La(NO_3)_3{\cdot}6H_2O$, $Al(NO_3)_3{\cdot}9H_2O$, and $Sr(CH_3COO)_2$ as starting materials. For the preparation of unsubstituted samples by the sol–gel process, lanthanum nitrate was first dissolved in CH_3COOH (50 ml 0.2 M) at 60 °C. To this solution, aluminium nitrate in 50 ml of distilled water was added and the resulting mixture was stirred for 2 h at the same temperature. For the preparation of Sr-substituted samples the appropriate amount of strontium acetate dissolved in 50 ml of 0.2 M CH_3COOH at 60 °C was added and the resulting mixture was stirred for 1 h at the same temperature. In a following step, 1,2-ethanediol (2 ml) as complexing agent was added to the reaction solution. After concentrating the solutions by a slow evaporation at 65 °C under stirring, the La(Sr)–Al–O acetate–nitrate–glycolate sols turned into white translucent gels. The oven dried (100 °C) gel powders were ground in an agate mortar and preheated for 3 h at 800 °C in air. Since the gels are very combustible, a slow heating rate (∼3–4 °C min^{-1}) especially between 100 and 400 °C was found to be essential. After an intermediate grinding in an agate mortar, the powders were additionally sintered in air for 10 h at 1000 °C.

The thermal decomposition processes of the precursor gels were studied in air atmosphere by thermogravimetric (TG) and differential thermal analyses (DTA) using a Setaram TG-DSC12 apparatus at a heating rate 10 °C min^{-1}. The infrared spectra were recorded on an EQUINOX 55/S/NIR FTIR spectrometer (4000–400 cm^{-1}). Samples were prepared as KBr pellets. Powder X-ray diffraction measurements were performed at room temperature on a Stoe-Cie Powder Diffraction System STADI P and a Siemens D-500 diffractometer operating with a Cu Kα radiation. Scanning electron microscopy (SEM) was used to study the morphology of the gels before and after the heat treatment. The SEM and energy dispersive X-ray (EDX) analysis were performed under vacuum in the specimen chamber of an EDX coupled scanning electron microscopes CAM SCAN S4 and CAMECA SX 100. ICP spectrometer Jobin Yvon 170 Ultrace (lateral observation, generator 40 MHz, output 1.0 kW, plasma gas flow 12 l min^{-1}, monochromator 1 m) was used for the determination of metals in the synthesized samples. The measurements were performed at the following lines: Al 309.271 and 396.152 nm; La 333.749 and 379.478 nm; Sr 407.771 and 421.552 nm.

3. Results and discussion

3.1. Synthesis of gels and calcined powders

In the recent years, the chemical synthesis routes have attracted significant attention as the low-temperature alternatives to the preparation method of multicomponent ceramic materials. We report here on the synthesis method, which is based on the in situ formation of metal complexes with chelating acetate and glycolate ligands. Previously we have demonstrated that the gelation time is a critical factor determining the nature of gels and is of crucial importance for the good properties of oxide materials [17]. A slow evaporation of the solution initiates condensation reactions resulting finally in resinous, transparent and homogeneous gels. Thus the sols, i.e. homogeneous mixtures of complexed metal ions, were heated to around 65 °C for several hours. Subsequently, the gels are charred (300–400 °C), calcined

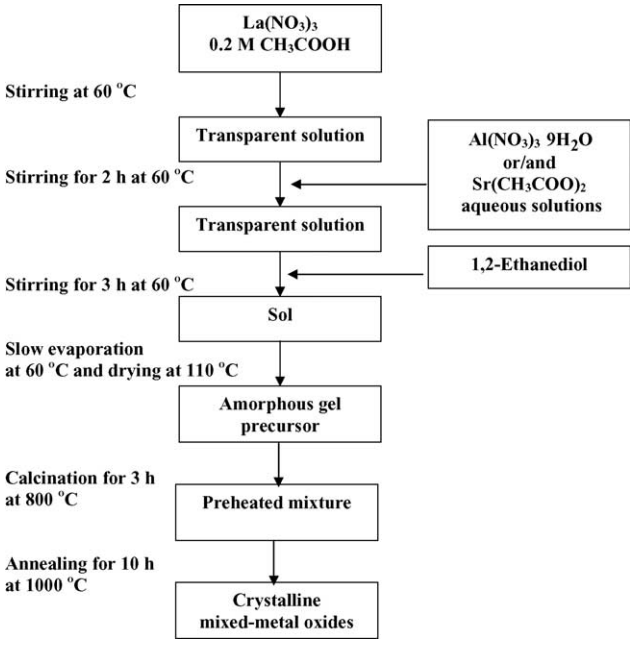

Fig. 1. Scheme of the steps involved in the sol–gel process used for the preparation of $LaAlO_3$ and $La_{1-x}Sr_xAlO_{3-\delta}$ ceramics.

(800 °C) and annealed (1000 °C) to obtain the oxide powders. A schematic diagram of the processing steps involved in the sol–gel synthesis of the mixed-metal $La_{1-x}Sr_xAlO_{3-\delta}$ aluminate ceramics is shown in Fig. 1.

3.2. Thermal analysis of precursor gels

The mechanism of the thermal decomposition in flowing air of the dried La–Al–O and La(Sr)–Al–O gels was studied by TG/DTA measurements. TG/DTA curves showed that in all cases (sample I–sample IV) the thermal decomposition proceeded in a similar way. TG/DTA profiles for two representative samples are shown in Figs. 2 and 3. Decomposition started below 120 °C with a loss of crystallization water and/or water from the coordination sphere of the metal complexes. In the temperature range of 120–550 °C the main decomposition occurs. The final weight loss (∼3.5–4.7%) on the TG curves of the gel

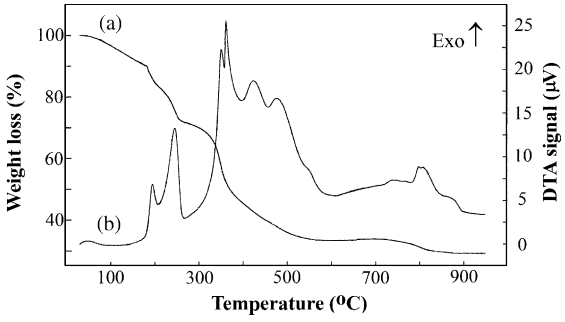

Fig. 2. TG/DTA profiles of the La(Sr)–Al–O precursor gel in which 25% of La was substituted by Sr.

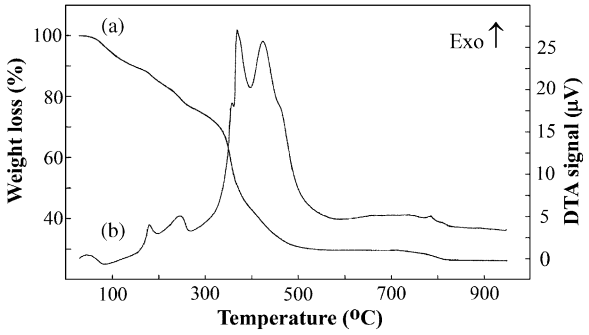

Fig. 3. TG/DTA profiles of the La(Sr)–Al–O precursor gel in which 75% of La was substituted by Sr.

samples I–IV was observed in the temperature range 760–890 °C. The thermal decomposition behaviour is associated with endothermic and exothermic effects in the DTA curves. The first decomposition step assignable to removal of adsorbed and chemisorbed water is indicated by broad endothermic peaks around 100 °C on the DTA curves. Exothermic peaks from 170 to 490 °C in the DTA curves are due to the pyrolysis processes occurring during further heating of the gel samples. The final weight loss observed on the TG curves is also accompanied by broad and weak exothermic peaks. These peaks probably correspond to the decomposition of the intermediate oxycarbonate $La_2O_2CO_3$ to the oxide which occurs in the temperature range 600–800 °C depending on the atmosphere used. According to the thermal analysis data the final annealing temperature for the preparation of $La_{1-x}Sr_xAlO_{3-\delta}$ ceramic oxides could vary from 900 to 1000 °C.

3.3. Elemental analysis

To check the metal contents in the dried La(Sr)–Al–O gel powders, the EDX method was applied. The average La:Sr:Al metal ratios for the prepared samples were calculated to be: 50(2):0:50(3) (sample I), 38(3):12(1):50(3) (sample II), 25(2):25(2):50(4) (sample III) and 13(1):37(3):50(2) (sample IV), with standard deviations of the distribution in parentheses. Thus, the syntheses yielded homogeneous precursors with compositions near to the desirable La:Sr:Al metal ratio 1:0:1, 0.75:0.25:1, 0.5:0.5:1, and 0.25:0.75:1 for the sample I to IV, respectively. Thus, the homogeneous gels were achieved by complexing metal ions with acetic acid and 1,2-ethanediol before gelation, and no component segregation or non-ideal stoichiometries, at the micrometer level, were observed in all of the cases.

The average metal ratios in the sintered (1000 °C) powders were also determined by the EDX analysis. These results are presented in Table 1. The EDX analyses of the different crystallites showed that the homogeneity of the samples depends on the nominal composition. In the case of a small amount of Sr (samples I and II) the metal

Table 1
Formulas of $La_{1-x}Sr_xAlO_3$ oxides calculated from EDX ($n = 5$) and ICP analysis data

Sample	Method of analysis	Major phase
I	EDX	$La_{0.9}Al_{1.0}O_{3-x}$
	ICP	$La_{0.8}Al_{1.0}O_{3-x}$
II	EDX	$La_{0.7}Sr_{0.3}Al_{1.0}O_{3-x}$
	ICP	$La_{0.6}Sr_{0.3}Al_{1.0}O_{3-x}$
III	EDX	$La_{0.5}Sr_{0.6}Al_{0.9}O_{3-x}$
	ICP	$La_{0.4}Sr_{0.5}Al_{1.0}O_{3-x}$
IV	EDX	$La_{0.2}Sr_{1.0}Al_{0.8}O_{3-x}$
	ICP	$La_{0.2}Sr_{0.8}Al_{1.0}O_{3-x}$

stoichiometry (La(Sr):Al = 1:1) consistent with the $La_{1-x}Sr_xAlO_{3-\delta}$ phase. The analyses of these two samples showed that La(Sr)–Al compositions approximated that of the dried gels. However, with a higher Sr substitutional level (samples III and IV) the syntheses yielded rather inhomogeneous products. EDX analyses in the SEM indicated that in the samples synthesized with a large amount of substituent, most of the particles were overstoichiometric in Sr and this seemed to be coupled with a decrease in the Al content. It is possible that the high Sr signals in the SEM analyses are due to neighboring strontium-rich grains. The observed lower amount of aluminium in the samples could be due to the possible formation of volatile intermediates during high-temperature treatment of the gels. However, the results of determination of metal content in the samples by ICP method (see Table 1) suggest that the calcination process does not influence the composition of the end products, i.e. the total amount of metals in the samples is consistent with the starting composition. On the other hand, the EDX results confirmed that various cations are inhomogeneously mixed in the individual grains of samples III and IV, and that there is considerable segregation of the components.

3.4. Infrared spectra

IR analysis of synthesized samples is important both for the control of the reaction process and of the properties of materials obtained. A special attention was paid to the IR spectra of the precursor gels. It is interesting to note that the IR spectra of La(Sr)–Al–O acetate–nitrate–glycolate gels are qualitatively the same regardless of strontium substitution level. A representative IR spectrum of the La–Al–O gel is shown in Fig. 4. The spectrum shows the characteristic absorption bands of vibrations in a number of functional groups, such as CH_2, CH_3, NO_3^-, CH–OH and –CO–OH [26,27]. These absorption bands are summarized in Table 2. The characteristic nitrate stretching frequencies at 1700–1600 cm^{-1} might be overlapped with the –CO–OH stretching. However, the peaks due to the stretch vibrations in NO_3^- at 1410–1360 cm^{-1} (strong bands) and 1270–1245 cm^{-1} (weak bands) [23,24] are evident. It is not possible to state that only one compound was formed,

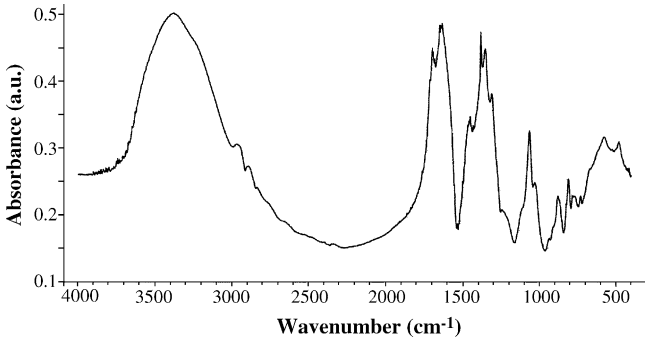

Fig. 4. IR spectrum of the La–Al–O precursor gel.

however, according to our IR results we suppose that the three ligands (acetate, nitrate and 1,2-ethanediol) are in the coordination sphere of the metals.

A broad absorption in the spectrum of the precursor gels at around 3400 cm^{-1} also indicates the presence of adsorbed water [17]. In the 820–400 cm^{-1} region of the IR spectrum, the observed specific peaks at 818, 789, 729, 772, 678, 578 and 484 cm^{-1} may be attributed to the characteristic M–O vibrations [27].

Fig. 5 shows the IR spectra of sintered $La_{1-x}Sr_xAlO_{3-\delta}$ ceramics obtained at 1000 °C. The $LaAlO_3$ spectrum (see Fig. 3a) displays only two frequencies at 660 and 435 cm^{-1} which are typical for the M–O (possibly La–O and Al–O stretching frequencies) vibrations for the perovskite structure compounds [27]. The IR spectra of Sr-substituted $La_{1-x}Sr_xAlO_{3-\delta}$ samples, however, change with an increasing Sr content, indicating the atomic-level reorganization. The strong bands of 660 and 435 cm^{-1} are replaced by several bands already at 50% substitutional level of Sr, which may be attributed to the stretching modes of different polyhedra in the oxide materials. Thus, the results of IR analysis indicate the formation of polyphasic crystalline material when concentration of Sr $x \geq 0.5$. In Fig. 5, the spectra of strontium substituted ceramic samples show that new peaks appear at 1448 cm^{-1} and in the region of 875–850 cm^{-1}. Moreover, the intensity of these peaks increases

Table 2
Characteristic absorption frequencies of the La–Al–O acetate–nitrate–glycolate gel in the 4000–800 cm^{-1} range

Group	Band (cm^{-1})	Remarks
>CH_2 and –CH_3	3000–2800	C–H stretching
	1460–1420	C–H deformations
–CH_2–OH	3400–3200	Strong
	1325–1270	Strong
	1100–1000	Medium
–CO–OH	3500–3200	Strong
	1720–1590	Strong
	1360–1350	Strong
	940–820	Medium
NO_3^-	1700–1600	Strong
	1410–1360	Strong
	1270–1245	Weak

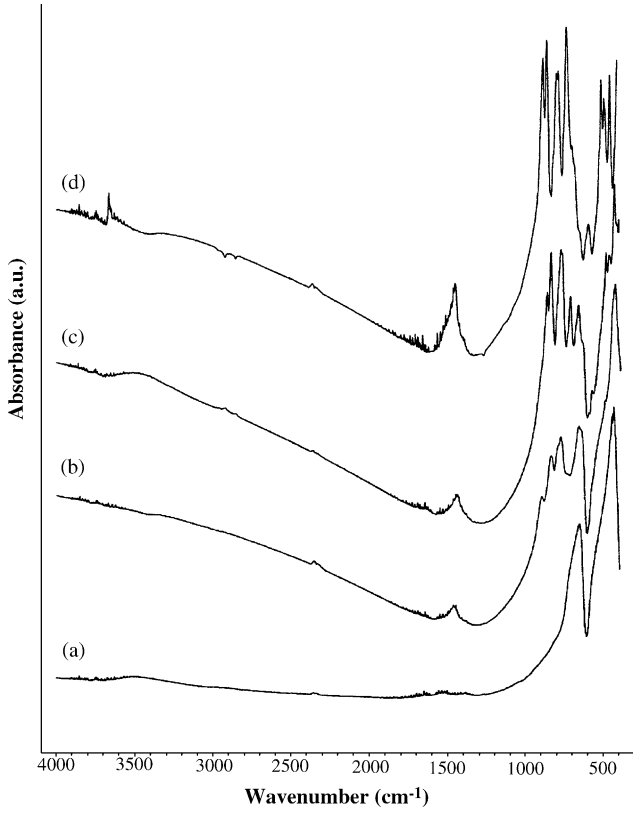

Fig. 5. IR spectra of different $La_{1-x}Sr_xAlO_{3-\delta}$ aluminates synthesized at 1000 °C: (a) $LaAlO_3$, (b) $La_{0.75}Sr_{0.25}AlO_{3-\delta}$, (c) $La_{0.50}Sr_{0.50}AlO_{3-\delta}$ and (d) $La_{0.25}Sr_{0.75}AlO_{3-\delta}$.

with increasing amount of strontium. The exact origin of this peak is not very clear. It is known, that typical carbonate vibrations are ~1470–1390 cm^{-1} (triply degenerated stretching mode) and ~880–850 cm^{-1} (doubly degenerated stretching mode) [26]. So, the bands at 1448, 875 and 851 cm^{-1} could be assigned to the metal carbonates formed as intermediates during high-temperature treatments. It is well known that aluminium carbonate ($Al_2(CO_3)_3$) decomposes relatively at low temperatures (~500 °C) [28]. Therefore, the carbonate peaks in the IR spectra of doped $La_{1-x}Sr_xAlO_3$ ceramic samples could be attributable to strontium carbonate ($SrCO_3$) and/or lanthanum oxycarbonate ($La_2O_2CO_3$). Because the intensity of 1448 cm^{-1} peak is relatively weak, it is likely that very little carbonate formed. However, the IR spectrum of undoped $LaAlO_3$ sample calcined at 1000 °C does not feature any characteristic carbonate bands.

3.5. Powder X-ray diffraction studies

The XRD patterns of the La–Al–O and La(Sr)–Al–O acetate–nitrate–glycolate gels were recorded in the region of $2\theta = 20–70^\circ$. The diffraction patterns of the obtained powders were broad due to the amorphous character of the synthesized systems. Again, all XRD patterns were qualitatively the same regardless of strontium substitutional

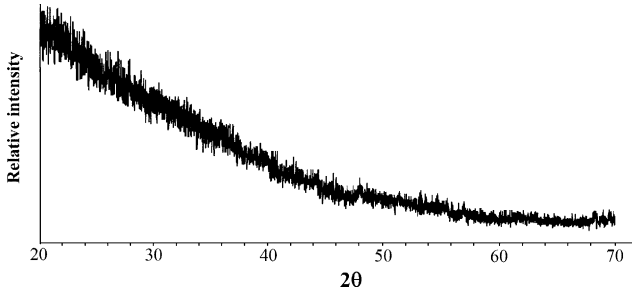

Fig. 6. X-ray diffraction pattern of the La(Sr)–Al–O precursor gel in which 50% of La was substituted by Sr.

level. The XRD pattern of the La(Sr)–Al–O dried gel in which 50% of La was substituted by Sr is presented in Fig. 6. In cases when the conditions of the sol–gel process are not optimized, a partial crystallization of the starting metal salts may occur. However, no peaks due to the crystallisation of metal salts or of any undesired or contaminating phase could be identified (see Fig. 6). These data show the individuality of the synthesized precursors. The powders remain amorphous to X-rays for calcination temperatures of up to 800 °C. The patterns for the products obtained at 800 °C only indicated an unidentified amorphous humps between $2\theta = 30–40^\circ$ and $2\theta = 55–65^\circ$. According to XRD analysis, syntheses performed at 900 °C yields crystalline samples having huge amount of different phases.

The XRD patterns of the La(Sr)–Al–O precursor powders calcined and sintered at 1000 °C are shown in Fig. 7. According to the XRD analysis, fully crystallized single-phase oxide $LaAlO_3$ with well pronounced perovskite

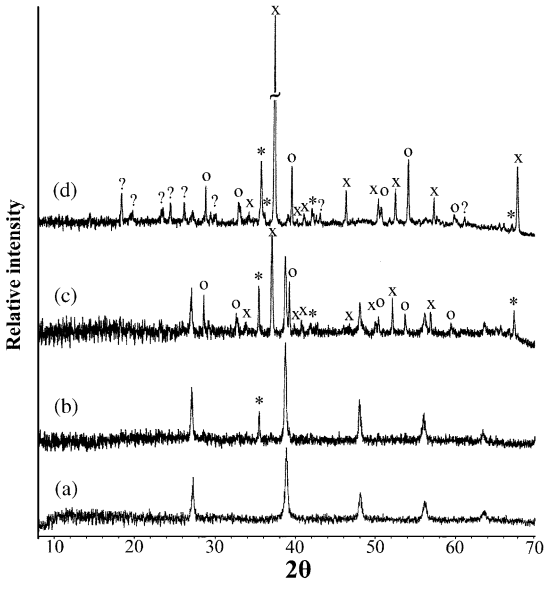

Fig. 7. X-ray diffraction patterns of the $La_{1-x}Sr_xAlO_{3-\delta}$ ceramic samples synthesized at 1000 °C: (a) $LaAlO_3$, (b) $La_{0.75}Sr_{0.25}AlO_{3-\delta}$, (c) $La_{0.50}Sr_{0.50}AlO_{3-\delta}$ and (d) $La_{0.25}Sr_{0.75}AlO_{3-\delta}$. The peaks other than those of the perovskite LAP phase are marked: $Sr_5Al_2O_8$ (*); $Sr_3Al_2O_6$ (x); $SrLaAlO_4$ (o); and unidentified phases (?).

crystal structure has formed (see Fig. 7a) (JCPDS file 31-22). The XRD pattern of the sample II (material with 25% of strontium) is presented in Fig. 7b. The XRD data confirm $La_{0.75}Sr_{0.25}AlO_{3-x}$ to be the main crystalline component. However, the formation of minor amount of impurity phase was also detected. The diffraction line at 35.5° 2θ could be attributed to the $Sr_5Al_2O_8$ phase. Fig. 7c shows the X-ray diffraction pattern of the $La_{0.50}Sr_{0.50}AlO_{3-\delta}$ ceramic sample. The diffraction lines assignable to the perovskite crystal structure at 27.5, 39.2, 48.5, 56.0 and 63.5 2θ are well pronounced in the diffractogram. However, the formation of the impurity phases such as $Sr_3Al_2O_6$, $Sr_5Al_2O_8$ and $SrLaAlO_4$ is also evident. With further increasing the Sr content, the formation of perovskite aluminate seems to be problematic. The impurity $Sr_3Al_2O_6$ phase was already the dominating component during the synthesis of $La_{0.25}Sr_{0.75}AlO_{3-\delta}$ ceramics (Fig. 7d). The main X-ray diffraction results are consistent with the crystallization process observed by the IR measurements. In contrast, the XRD powder patterns show no evidence for the formation of crystalline carbonate species. Moreover, these observations are thoroughly supported by the scanning electron microscopy studies (see later). The broad peaks in the resulting powder patterns and poor intensities suggest that a considerable amount of the material is either amorphous or nanocrystalline [28].

3.6. Scanning electron microscopy

The typical scanning electron micrographs of La(Sr)–Al–O gels display amorphous particles forming ~20–50 μm sized highly porous cloud-like agglomerates, and no faceted grains were observed in all of the cases. A representative SEM photograph of the precursor gel (sample II) is shown in Fig. 8. This observed morphology was qualitatively the same in different gels regardless of their chemical composition.

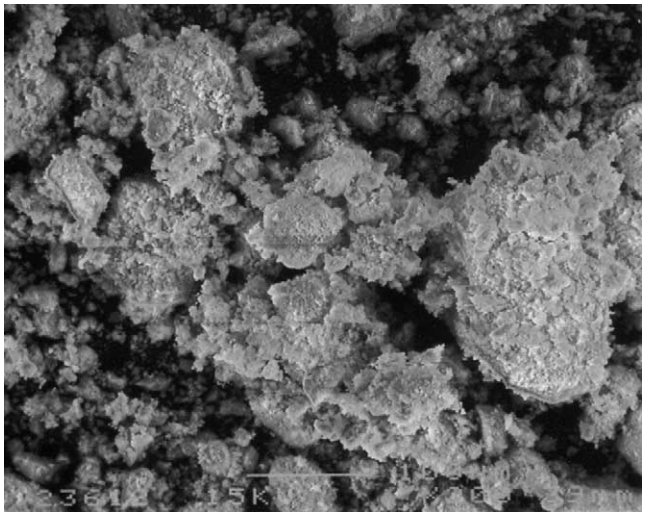

Fig. 8. Scanning electron micrograph of the La(Sr)–Al–O precursor gel in which 25% of La was substituted by Sr. Magnification 300×.

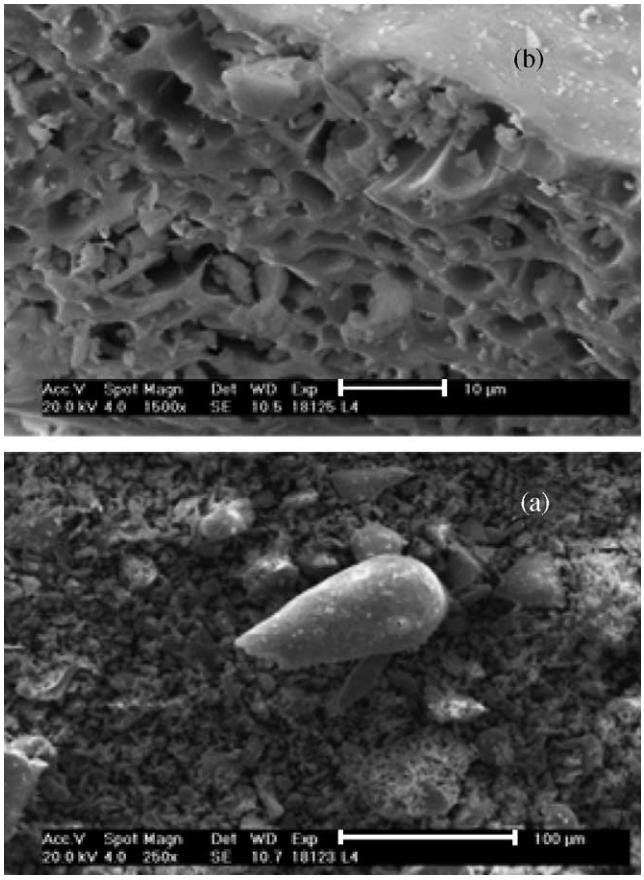

Fig. 9. Scanning electron micrographs of $LaAlO_3$ ceramics at two magnifications: (a) 250× and (b) 1500×.

The SEM images of the calcined $LaAlO_3$ sample exhibit clustered grains made up of several tiny crystallites with a defined microstructure (Fig. 9). Some individual particles seem to be nano-sized plate-like crystals and they are partially fused to form hard agglomerates (see Fig. 9b). It can be also seen from Fig. 9 that the LAP solids are composed of grains with no regular size, i.e. the SEM images revealed agglomerated grains of different size ranging from ~500 nm to 25 μm. The particle size does not change and no progressive change in morphology was observed with strontium substitution. Fig. 10 shows the surface features of the $La_{0.75}Sr_{0.25}AlO_{3-\delta}$ and $La_{0.50}Sr_{0.50}AlO_{3-\delta}$ powders calcined at 1000 °C. From these SEM images it is evident that the $La_{1-x}Sr_xAlO_{3-\delta}$ powders are also composed of plate-like crystallites having a quite different size and the tendency to form agglomerates.

Fig. 11 shows the SEM micrographs (back scattered electron (BSE) images) of synthesized $La_{1-x}Sr_xAlO_{3-\delta}$ powders. As seen, in the backscattered electron mode the light or dark regions cannot be identified for the $LaAlO_3$ sample (Fig. 11a). The similar situation is observed for the $La_{0.75}Sr_{0.25}AlO_{3-\delta}$ and $La_{0.50}Sr_{0.50}AlO_{3-\delta}$ samples, whose BSE micrographs are presented in Fig. 11b and c, respectively. However, the appearance of a small number of dark spots within the gray matrix is evident. Since the

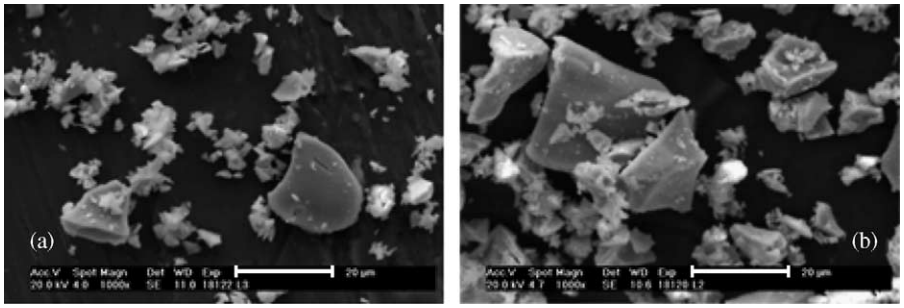

Fig. 10. Scanning electron micrographs of (a) $La_{0.75}Sr_{0.25}AlO_{3-\delta}$ and (b) $La_{0.50}Sr_{0.50}AlO_{3-\delta}$ ceramics. Magnification 1000×.

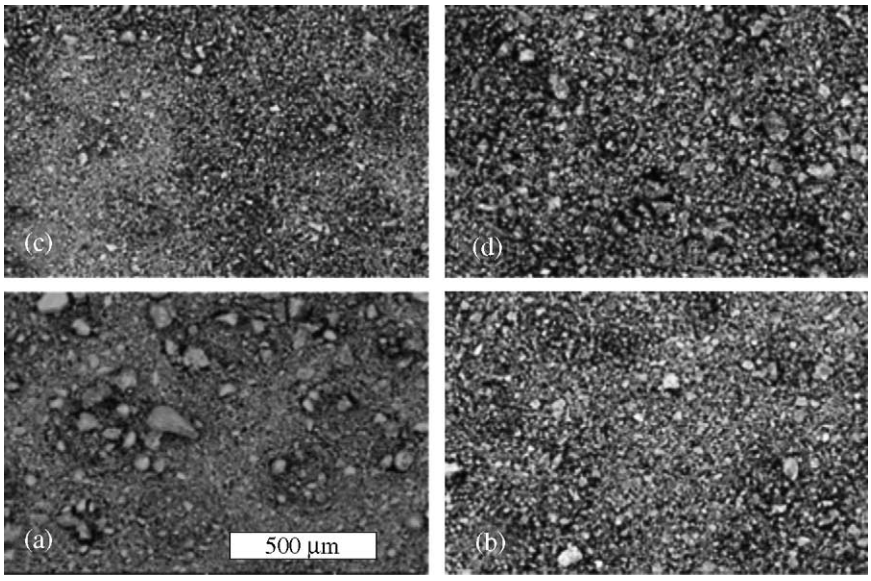

Fig. 11. Scanning electron micrographs of $La_{1-x}Sr_xAlO_{3-\delta}$ aluminates synthesized at 1000 °C ((a) $LaAlO_3$, (b) $La_{0.75}Sr_{0.25}AlO_{3-\delta}$, (c) $La_{0.50}Sr_{0.50}AlO_{3-\delta}$ and (d) $La_{0.25}Sr_{0.75}AlO_{3-\delta}$) in back scattered electron mode.

brightness of the specimen in BSE is homogeneous over the entire measured area, the most of the material is finely divided, i.e. the distribution of its chemical elements is highly uniform. Fig. 11d shows the distribution of white, gray and black regions through the whole picture confirming the formation of multiphasic materials during the synthesis of high-level strontium substituted $La_{0.25}Sr_{0.75}AlO_{3-\delta}$ ceramics.

4. Conclusions

From the present study it might be concluded that homogeneous gels in the La(Sr)–Al–O system were prepared by the complexation of metal ions with 1,2-ethanediol followed by a controlled hydrolysis in aqueous media. The obtained gels have been used for the low-temperature synthesis of nano-scale lanthanum aluminate (LAP, $LaAlO_3$) and strontium substituted lanthanum aluminate ($La_{1-x}Sr_xAlO_{3-\delta}$) ceramics. The present study demonstrates the versatility of the solution method to yield a monophasic LAP sample at low sintering temperature (1000 °C) when compared to the temperature required for the solid-sate synthesis (>1400–1600 °C). Moreover, the proposed sol–gel method of preparation of LAP in aqueous media is inexpensive and thus appropriate for the large-scale production of such type ceramics. Also, the Sr-substituted LAP ceramics have been successfully obtained by this method. To our knowledge, $La_{1-x}Sr_xAlO_{3-\delta}$ ($x \leq 0.50$) solid solutions with the perovskite structure were prepared by a soft sol–gel chemistry approach for the first time. Ultrafine particles of different crystallite dimensions (from ~500 nm to 25 μm) can be formed in 10 h at 1000 °C. Recent studies have shown that highly transparent aluminate ceramics with optical transmittance comparable to single crystal could be obtained from the compacts of polycrystalline materials. In the view of the above results and the increasing importance of the nanomaterials, the nanocrystalline LAP and Sr-substituted LAP phases show a considerable application potential.

Acknowledgements

The authors from Vilnius University gratefully acknowledge the financial support from the Lithuanian State Science and Education Foundation under project MODELITA (No. C-03048). Financial support by the GACR (203/01/1533) is gratefully acknowledged. The authors are indebted to E. Garskaite for technical assistance.

References

[1] M. Marezio, P.D. Dernier, J.P. Remeika, The crystal structures of orthorhombic $SmAlO_3$ and of trigonal $NdAlO_3$, J. Solid State Chem. 4 (1972) 11.

[2] P. Padmini, T.R.N. Kutty, Wet chemical syntheses of ultrafine multicomponent ceramic powders through gel to crystallite conversion, J. Mater. Chem. 4 (12) (1994) 1875.

[3] C.P. Joshi, S.V. Moharil, Self heat generating synthesis of tri-colour lamp phosphors, Bull. Mater. Sci. 20 (5) (1997) 707.

[4] B.J. Kennedy, C.J. Howard, A.K. Prodjosantoso, B.C. Chakoumakos, Neutron powder diffraction study of the rhombohedral to cubic phase transition in the series $La_{1-x}Pr_xAlO_3$, Appl. Phys. A—Mater. Sci. Process. 74 (2002) 1660.

[5] R. Guo, D. Guo, Y. Chen, Z. Yang, Q. Yuan, In situ formation of $LaAl_{11}O_{18}$ rodlike particles in ZTA ceramics and effect on the mechanical properties, Ceram. Int. 28 (7) (2002) 699.

[6] J. Zhang, L. Zhang, Z. Tang, Z. Zhang, T. Wang, Luminescent properties of $(Ce_{0.67}Tb_{0.33})Mn_xMg_{1-x}Al_{11}O_{19}$ phosphor in VUV region, Ceram. Int. 29 (5) (2003) 583.

[7] M.J. Jackson, W. O'Neill, Laser micro-drilling of tool steel using Nd:YAG lasers, J. Mater. Process. Technol. 142 (2) (2003) 517.

[8] B. Jancar, D. Suvorov, M. Valant, G. Drazic, Characterization of $CaTiO_3$–$NdAlO_3$ dielectric ceramics, J. Eur. Ceram. Soc. 23 (9) (2003) 1391.

[9] M. Malinowski, R. Piramidowicz, Z. Frukacz, G. Chadeyron, R. Mahiou, M.F. Joubert, Spectroscopy and upconversion processes in $YAlO_3$:Ho^{3+} crystals, Opt. Mater. 12 (4) (1999) 409.

[10] M. Yada, M. Ohya, M. Machida, T. Kijima, Synthesis of porous yttrium aluminium oxide templated by dodecyl sulfate assemblies, Chem. Commun. 18 (1998) 1941.

[11] D.A. Atwood, B.C. Yearwood, The future of aluminum chemistry, J. Organomet. Chem. 600 (1/2) (2000) 186.

[12] M. Nieminen, T. Sajavaara, E. Rauhala, M. Putkonen, L. Niinistö, Surface-controlled growth of $LaAlO_3$ thin films by atomic layer epitaxy, J. Mater. Chem. 11 (12) (2001) 2340.

[13] P.D. Tall, C. Coupeau, J. Rabier, Indentation-induced twinning in $LaAlO_3$ single crystals: an atomic force microscopy study, Scripta Mater. 49 (9) (2003) 903.

[14] I. Zvereva, Y. Smirnov, V. Gusarov, V. Popova, J. Choisnet, Complex aluminates $RE_2SrAl_2O_7$ (RE = La, Nd, Sm–Ho): cation ordering and stability of the double perovskite slab-rocksalt layer P-2/RS intergrowth, Solid State Sci. 5 (2) (2003) 343.

[15] A. Douy, M. Capron, Crystallization of spray-dried amorphous precursors in the SrO–Al_2O_3 system: a DSC study, J. Eur. Ceram. Soc. 23 (12) (2003) 2075.

[16] Y. Liu, C.N. Xu, Influence of calcining temperature on photoluminescence and triboluminescence of europium-doped strontium aluminate particles prepared by sol–gel process, J. Phys. Chem. B 107 (17) (2003) 3991.

[17] A. Baranauskas, D. Jasaitis, A. Kareiva, Characterization of sol–gel process in the Y–Ba–Cu–O acetate–tartrate system using IR spectroscopy, Vibr. Spectrosc. 28 (2) (2002) 263.

[18] T. Aitasalo, J. Holsa, H. Jungner, M. Lastusaari, J. Niittykoski, Mechanisms of persistent luminescence in Eu^{2+}, RE^{3+} doped alkaline earth aluminates, J. Lumin. 94 (2001) 59.

[19] D. Wang, Q.R. Yin, Y.X. Li, M.Q. Wang, Concentration quenching of Eu^{2+} in $SrO{\cdot}Al_2O_3$:Eu^{2+} phosphor, J. Lumin. 97 (1) (2002) 1.

[20] J. Sanchez-Benitez, A. de Andres, M. Marchal, E. Cordoncillo, M.V. Regi, P. Escribano, Optical study of $SrAl_{1.7}B_{0.3}O_4$:Eu, R (R = Nd, Dy) pigments with long-lasting phosphorescence for industrial uses, J. Solid State Chem. 171 (1/2) (2003) 273.

[21] T. Aitasalo, J. Holsa, M. Lastusaari, J. Legendziewicz, J. Niittykoski, Persistent luminescence of Eu^{2+} and Na^+ doped alkaline earth aluminates, Radiat. Eff. Def. Solids 158 (1–6) (2003) 89.

[22] A.A. Bosak, S.V. Samoilenkov, O.Yu. Gorbenko, A.N. Botev, A.R. Kaul, Self-tuning MOCVD approach to the growth of very smooth $La_{1-x}Pb_xMnO_3$ thin films, Int. J. Inorg. Mater. 3 (8) (2001) 1097.

[23] J. Livage, M. Henry, C. Sanchez, Sol–gel chemistry of transition metal oxides, Prog. Solid State Chem. 18 (4) (1988) 259.

[24] C.J. Brinker, G.W. Scherrer, Sol–Gel Science: The Physics and Chemistry of Sol–Gel Processing, Academic Press, New York, 1990.

[25] C. Sanchez, G.J.D.A.A. Soler-Illia, F. Ribot, D. Grosso, Design of functional nano-structured materials through the use of controlled hybrid organic–inorganic interfaces, C. R. Chim. 6 (8–10) (2003) 1131.

[26] K. Nakamoto, Infrared and Raman Spectra of Inorganic and Coordination Compounds, John Wiley & Sons, New York, 1986.

[27] B. Schrader (Ed.), Infrared Raman Spectroscopy: Methods and Applications, VCH, Weinheim, 1995.

[28] Y. Liu, Z.-F. Zhang, B. King, J. Halloran, R.M. Laine, Synthesis of yttrium aluminium garnet from yttrium and aluminium isobutyrate precursors, J. Am. Ceram. Soc. 79 (2) (1996) 385.